

# Thinking Like a Radiologist: A Dataset for Anatomy-Guided Interleaved Vision Language Reasoning in Chest X-ray Interpretation

Yichen Zhao<sup>1†</sup>, Zelin Peng<sup>1†</sup>, Piao Yang<sup>2</sup>, Xiaokang Yang<sup>1</sup>, and Wei Shen<sup>1( $\boxtimes$ )</sup>

<sup>1</sup> MoE Key Lab of Artificial Intelligence, AI Institute, School of Computer Science, Shanghai Jiao Tong University, Shanghai, China

<sup>2</sup> Department of Radiology, The First Affiliated Hospital, Zhejiang University School of Medicine, Hangzhou, Zhejiang, China

**Abstract.** Radiological diagnosis is a perceptual process in which careful visual inspection and language reasoning are repeatedly interleaved. Most medical large vision language models (LVLMs) perform visual inspection only once and then rely on text-only chain-of-thought (CoT) reasoning, which operates purely in the linguistic space and is prone to hallucination. Recent methods attempt to mitigate this issue by introducing visually related coordinates, such as bounding boxes. However, these remain a pseudo-visual solution: coordinates are still text and fail to preserve rich visual details like texture and density. Motivated by the interleaved nature of radiological diagnosis, we introduce **MMRad-IVL-22K**, the first large-scale dataset designed for natively interleaved visual language reasoning in chest X-ray interpretation. MMRad-IVL-22K reflects a repeated cycle of reasoning and visual inspection workflow of radiologists, in which visual rationales complement textual descriptions and ground each step of the reasoning process. MMRad-IVL-22K comprises **21,994** diagnostic traces, enabling systematic scanning across **35** anatomical regions. Experimental results on advanced closed-source LVLMs demonstrate that report generation guided by multimodal CoT significantly outperforms that guided by text-only CoT in clinical accuracy and report quality (e.g., **6%** increase in the RadGraph metric), confirming that high-fidelity interleaved vision language evidence is a non-substitutable component of reliable medical AI. Furthermore, benchmarking across seven state-of-the-art open-source LVLMs demonstrates that models fine-tuned on MMRad-IVL-22K achieve superior reasoning consistency and report quality compared with both general-purpose and medical-specific LVLMs. The project page is available at [https://github.com/qiuzyc/thinking\\_like\\_a\\_radiologist](https://github.com/qiuzyc/thinking_like_a_radiologist).

**Keywords:** Radiological Diagnosis · Multimodal Chain-of-Thought · Interleaved Vision Language Reasoning

---

$\boxtimes$  Corresponding Author: [wei.shen@sjtu.edu.cn](mailto:wei.shen@sjtu.edu.cn)

$\dagger$  Indicates equal contribution.

## 1 Introduction

The radiological diagnostic process is fundamentally an act of active perception. When a radiologist interprets a Chest X-ray (CXR), the diagnostic process is never a static and direct image-to-text translation; rather, it is a multi-step, interleaved diagnostic trace where careful visual inspection drives deductive reasoning, and intermediate deductions trigger renewed visual inspection [22]. For instance, when a radiologist identifies an opacity, they actively zoom in to scrutinize the lung texture, and mentally isolate the region to verify consolidation versus atelectasis. This interleaved “seeing and thinking” integrates localized visual evidence into a coherent clinical rationale, thereby ensuring that every diagnostic conclusion is grounded in verifiable visual evidence.

Despite the rapid advancement of Large Vision Language Models (LVLMs) in medical report generation, current state-of-the-art methods lack such an interleaved perceptual process. While recent works such as LVMed-R2 [25] and MRG-R1 [26] have enhanced diagnostic logic via “reflexive thinking” and reinforcement learning (RL), they still perform visual inspection only once at the onset. Consequently, the subsequent reasoning process operates purely in a linguistic space through text-only Chain-of-Thought (CoT). As this text-only CoT extends, the generation becomes increasingly decoupled from the initial visual features and overly conditioned on preceding tokens, leading to hallucinations [24].

To mitigate this issue, recent approaches such as BoxMed-RL [12] and datasets like GEMeX [18] and GEMeX-ThinkVG [17] train models to predict visually related bounding box coordinates (e.g., [x1, y1, x2, y2]). While this aligns text with spatial regions, we argue that coordinates are insufficient for visual perception, because these coordinates are essentially still texts. It indicates location but discards the critical features such as texture, density, and margin sharpness in that region. For instance, in BoxMed-RL [12], the model outputs bounding boxes as a final answer or a reward signal, but it does not natively consume the visual information within bounding boxes to inform subsequent reasoning steps.

Given that text-only CoT is inherently constrained, we propose that to truly “see and think” like a radiologist, a model must move beyond text-only CoT to natively interleaved vision language reasoning. Motivated by the interleaved nature of radiological diagnosis, we introduce MMRad-IVL-22K, the first large-scale multimodal dataset designed for natively interleaved visual language reasoning in chest X-ray interpretation. MMRad-IVL-22K provides 21,994 high-quality multimodal diagnostic traces derived from MIMIC-CXR [13] dataset. MMRad-IVL-22K instantiates a cyclical workflow of reasoning and visual inspection, where visual rationales (localized visual evidence) complement textual descriptions to ground the diagnostic process. Leveraging this dataset, we conduct two experiments. First, we validate the efficacy of multimodal CoT against text-only CoT. The results demonstrate that multimodal CoT guides state-of-the-art closed-source LVLMs to generate more accurate radiological reports, yielding a 6% improvement in the RadGraph [11] metric. Second, we train Anole-RadCoT using our dataset, a model capable of outputting interleaved multimodal diagnostic traces. Anole-RadCoT achieves superior reasoning consistency and report

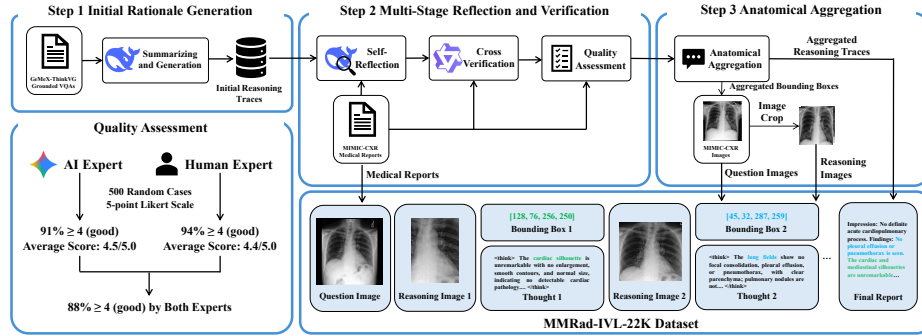


**Fig. 1. Pipeline of MMRad-IVL-22K.** (1) Initial interleaved reasoning traces and region-text correspondences are generated and summarized based on GEMeX-ThinkVG via DeepSeek-v3. (2) Multi-stage verification is conducted through DeepSeek-v3 self-reflection, Qwen2.5-72B cross-auditing, and domain expert adjudication to ensure clinical fidelity. (3) Refined rationales and bounding boxes are aggregated into major anatomical categories. (4) Localized reasoning images are cropped and assembled with textual traces and medical reports to form the final interleaved MMRad-IVL-22K dataset.

quality compared with existing state-of-the-art open-source general and medical LLMs. These findings underscore that high-fidelity interleaved vision-language evidence is an indispensable component of reliable medical AI, as multimodal CoT aligns more closely with clinical workflows to ensure higher diagnostic accuracy. Consequently, MMRad-IVL-22K provides a valuable resource to facilitate the development and evaluation of unified multimodal LLMs in the medical domain.

## 2 MMRad-IVL-22K Dataset

In this section, we first introduce the construction pipeline of MMRad-IVL-22K (Sec. 2.1), then present the statistical information of the dataset (Sec. 2.2). Finally, we compare our dataset with existing medical radiology datasets (Sec. 2.3).

### 2.1 Data Construction

**Initial Interleaved Rationale Generation.** As shown in Figure 1, we leverage GEMeX-ThinkVG [17] as the foundation for the thinking trace construction due to its expert-verified reasoning traces and accurate anatomical bounding boxes. By summarizing these CoT steps via DeepSeek-v3 [16], we establish an initial “see and think” correspondence, pairing each textual rationale with its corresponding anatomical region.

**Multi-Stage Reflection and Verification.** To ensure the reliability of the reasoning traces, we implement a multi-stage verification pipeline. Initially, DeepSeek-

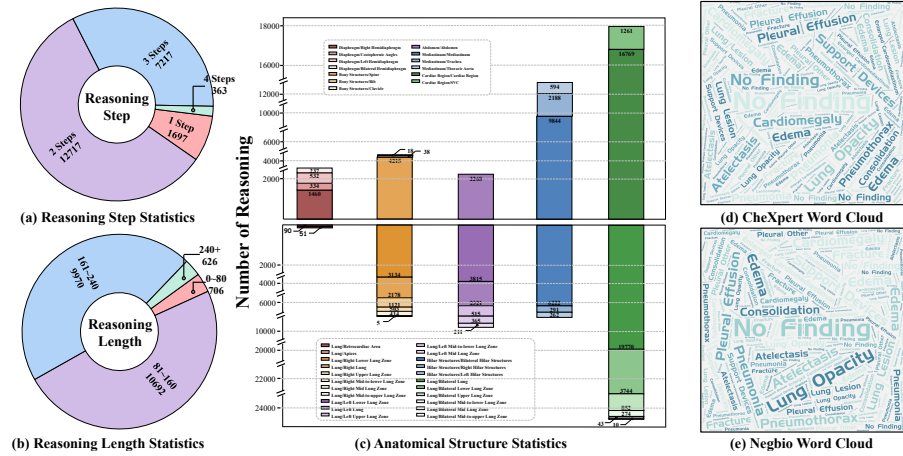


**Fig. 2. Statistical overview of MMRad-IVL-22K.** (a-b) Distribution of reasoning steps and rationale lengths. (c) Fine-grained anatomical structures. (d-e) Clinical characteristics extracted across the dataset.

v3 [16] refines the initial reasoning traces via self-reflection. Since the GEMeX-ThinkVG [17] dataset is derived from MIMIC-CXR [13], it leverages the available ground truth reports to identify and rectify descriptions that contradict the clinical findings, thereby mitigating hallucinations. Subsequently, to reduce single-model bias, Qwen2.5-72B [4] serves as an independent AI evaluator, cross-verifying the logical consistency of each trace to uncover potential discrepancies overlooked by Deepseek-v3 [16]. Any new inconsistencies flagged during this audit are adjudicated by a human domain expert to determine the necessary revisions. To validate clinical fidelity, 500 randomly selected cases are independently and blindly evaluated by a human domain expert and an AI expert (Gemini-3.0-pro [8]) using a 5-point Likert scale with pre-defined detailed criteria. The cases receive high mean scores of 4.4 and 4.5 from the human and the AI evaluator, respectively. Notably, approximately 94% and 91% of cases are rated  $\geq 4$  (good), respectively, and over 88% of cases are rated  $\geq 4$  (good) by both evaluators. These results confirm that our synthetic traces effectively emulate the diagnostic logic of human radiologists while maintaining high clinical fidelity and aligned language style with the ground truth reports.

**Anatomical Aggregation and Dataset Assembly.** To ensure structural consistency of CoT, we aggregate the refined traces into major anatomical categories, including mediastinal, lung, bone, and other regions. We merge the textual descriptions and bounding boxes within each group and crop localized reasoning images from the original MIMIC-CXR [13] images. The final MMRad-IVL-22K dataset is then assembled by combining these localized images, descriptions, and coordinates into interleaved reasoning chains, while the original ground truth reports serves as the diagnostic conclusion. This results in a comprehensive natively interleaved vision language format.

**Table 1.** Comparison of **MMRad-IVL-22K** with other medical radiology datasets. Grd. refers to grounding. Diag. refers to diagnosis.

Dataset	Task	Grd.	Reasoning Trace	CoT Modality	Trace Structure
MIMIC-CXR [13]	Diag.	✗	✗	—	—
EHRXQA [3]	VQA	✗	✗	—	—
RadGenome [31]	Diag.	✓	✗	—	—
GEMeX-ThinkVG [17]	VQA	✓	✓	Text	Single-turn
<b>MMRad-IVL-22K (ours)</b>	<b>Diag.</b>	<b>✓</b>	<b>✓</b>	<b>Text + Img</b>	<b>Multi-step</b>

## 2.2 Data Statistics

As shown in Figure 2, the MMRad-IVL-22K dataset comprises 21,994 high-quality interleaved vision language reasoning traces derived from real-world chest X-ray scans. On the anatomical side, the dataset is categorized into 4 major domains: Lung, Mediastinal, Bone, and Others. Regarding the reasoning depth, each report is annotated with a multi-step interleaved chain averaging 2.3 steps and localized reasoning images (Figure 2 (a)), providing fine-grained visual evidence for corresponding textual observations. The average lengths of thinking rationales are 160 words (Figure 2 (b)). Although these traces are grouped into four clinical domains for structural consistency, their content maintains high specificity across 35 fine-grained anatomical sub-regions (Figure 2 (c)). Beyond spatial diversity, the dataset captures a comprehensive range of clinical characteristics (Figure 2 (d, e)), representing a balanced diagnostic spectrum from baseline healthy cases to various thoracic abnormalities. Notably, 100% of the reasoning steps are grounded in specific anatomical regions, highlighting the high mapping precision and explainability of our dataset.

## 2.3 Data Comparison

In Table 1, we compare MMRad-IVL-22K with existing medical radiology datasets. Compared with foundational datasets, MMRad-IVL-22K presents a significantly more rigorous challenge. A critical distinction lies in our natively interleaved CoT modality (Text + Image). Unlike text-only CoT datasets such as GEMeX-ThinkVG [17], which is limited to single-turn VQA textual rationales, MMRad-IVL-22K requires models to natively generate multi-step interleaved textual thoughts and visual rationales during the thinking process. This integration of multimodal understanding and generation tasks aligns with the latest trend of unified multimodal foundation models.

## 3 Experiments

In this section, we first evaluate the technical route of multimodal CoT reasoning in Sec. 3.1. Building on these findings, in Sec. 3.2, we leverage the MMRad-IVL-

**Table 2.** Performance comparison between text-only and multimodal CoTs for medical report generation. The multimodal approach consistently outperforms the unimodal baseline across all NLG and CE metrics. Abbreviations: B-n: BLEU-n; MTR: METEOR; R-L: ROUGE-L; RG: RadGraph [11]. **Bold** denotes the best-performing outcome.

Model	CoT Strategy	NLG Metrics						CE Metrics		
		B-1	B-2	B-3	B-4	MTR	R-L	RG <sub>e</sub>	RG <sub>er</sub>	RG <sub>ber</sub>
GPT-5 [23]	Text-only	0.217	0.112	0.057	0.022	0.193	0.166	0.316	0.288	0.215
	Multimodal	<b>0.226</b>	<b>0.199</b>	<b>0.061</b>	<b>0.026</b>	<b>0.201</b>	<b>0.172</b>	<b>0.333</b>	<b>0.304</b>	<b>0.229</b>
Gemini-3.0-Flash [7]	Text-only	0.257	0.139	0.076	0.034	0.217	0.200	0.332	0.305	0.225
	Multimodal	<b>0.274</b>	<b>0.155</b>	<b>0.088</b>	<b>0.042</b>	<b>0.224</b>	<b>0.212</b>	<b>0.357</b>	<b>0.329</b>	<b>0.248</b>
Claude-Haiku-4.5 [2]	Text-only	0.187	0.098	0.048	0.018	0.172	0.150	0.320	0.295	0.222
	Multimodal	<b>0.199</b>	<b>0.109</b>	<b>0.057</b>	<b>0.023</b>	<b>0.179</b>	<b>0.159</b>	<b>0.343</b>	<b>0.316</b>	<b>0.242</b>
Qwen3-VL-Plus [29]	Text-only	0.218	0.104	0.050	0.019	0.185	0.161	0.306	0.277	0.202
	Multimodal	<b>0.227</b>	<b>0.110</b>	<b>0.055</b>	<b>0.022</b>	<b>0.188</b>	<b>0.165</b>	<b>0.320</b>	<b>0.291</b>	<b>0.212</b>

22K dataset to fine-tune a unified model, resulting in Anole-RadCoT. Anole-RadCoT generates interleaved multimodal CoT and achieves superior performance in generation, grounding, and semantic understanding. Moreover, we compare report quality against existing LVLMs, further demonstrating the value of our dataset for training high-performance systems. Finally, Sec. 3.3 presents a qualitative analysis.

### 3.1 Value Analysis of Multimodal CoT

General frontier models (GPT-5 [23], Gemini-3-Flash [7], Claude-Haiku-4.5 [2], Qwen3-VL-Plus [29]) have demonstrated strong capabilities in multimodal reasoning tasks. To investigate whether integrating localized visual evidence with textual descriptions improves medical report generation compared to using text alone, we design a controlled experiment comparing text-only and multimodal CoTs. We focus on comparing two conditions:

- **Text-only**:  $\langle$ full image $\rangle + \langle$ regional text $\rangle$
- **Multimodal**:  $\langle$ full image $\rangle + \langle$ regional text $\rangle + \langle$ regional vision $\rangle$

where  $\langle$ full image $\rangle$  indicates full CXR image,  $\langle$ regional text $\rangle$  and  $\langle$ regional vision $\rangle$  indicate the textual description and localized image of one of the local anatomical regions in the thinking trace.

**Evaluation Metrics and Data Subsampling.** Following established protocols [19,20], we evaluated model performance on both NLG Metrics and CE Metrics. To ensure computational efficiency while maintaining data representativeness, we conducted experiments on a 5% subset (1097 samples in total) of the full dataset. This subset was randomly selected through stratified sampling based on the number of reasoning steps.

**Results and Analysis.** As shown in Table 2, multimodal CoT demonstrates superiority across all evaluated metrics. These gains demonstrate that visual

**Table 3.** Benchmark results for Understanding-Only and Unified LVLMs. Abbreviations: Params.: activated parameters; Consist.: consistency; G: general; M: medical. Gen.: generation consistency. Sem.: semantic consistency. Grd.: grounding consistency. **Bold** denotes the best-performing outcome, and underline indicates the second-best. <sup>†</sup> Part of our test set is present in the model’s training data.

Models	Params.	Domain	Consist. Metrics			NLG Metrics			CE Metrics		
			Gen.	Sem.	Grd.	B-1	MTR	R-L	RG <sub>er</sub>	RG <sub>ber</sub>	
<b>Understanding-Only Large Language Models</b>											
Deepseek-VL2 [28]	4.5B	G	—	—	—	0.365	0.104	0.081	0.098	0.061	0.033
Qwen3-VL [29]	8B	G	—	—	—	<u>0.569</u>	0.154	0.112	0.118	0.121	0.069
InternVL3.5 [27]	8B	G	—	—	—	0.527	0.179	0.122	<u>0.136</u>	0.122	0.071
LLaVA-Med-1.5 [15]	7B	M	—	—	—	0.407	0.127	0.069	0.097	0.054	0.021
MiniGPT-Med <sup>†</sup> [1]	7B	M	—	—	—	0.099	0.145	0.103	0.131	<b>0.180</b>	<b>0.127</b>
<b>Unified Large Language Models</b>											
Bagel [6]	7B	G	<u>0.311</u>	1.082	0.495	0.118	0.123	0.113	0.112	0.066	
UniMedVL [21]	14B	M	0.181	<u>1.131</u>	0.458	0.154	<u>0.129</u>	0.123	0.125	0.073	
<b>Anole-RadCoT (ours)</b>	7B	M	<b>0.482</b>	<b>1.226</b>	<b>0.643</b>	<b>0.193</b>	<b>0.153</b>	<b>0.160</b>	<u>0.151</u>	<u>0.097</u>	

evidence provides essential information that textual descriptions alone cannot convey, enabling models to produce more clinically accurate and detailed reports. These results underscore the value of our natively interleaved dataset structure, confirming that high-fidelity interleaved vision language evidence is a non-substitutable component of reliable medical AI.

### 3.2 Benchmarking LVLMs on MMRad-IVL-22K

**Data Split.** We employ a randomly stratified data split based on the number of reasoning steps. Specifically, we randomly sample 5% to construct the benchmark set, while the remaining 95% are utilized for training.

**A Baseline Finetuned on MMRad-IVL.** We fine-tune the Anole-Zebra-CoT [14] model on the MMRad-IVL dataset, leveraging the training framework established by Chern et al. [5]. We employ LoRA [9] on the query, key, and value projections of the attention modules with a rank  $r = 16$  and a scaling factor  $\alpha = 32$ . The optimization process span 50,000 steps on two NVIDIA H800 GPUs. We utilize a learning rate of  $1 \times 10^{-5}$  and a batch size of 2.

**Existing LVLMs.** To further investigate the generalization capabilities of existing models and the complexity of MMRad-IVL, we benchmark seven additional state-of-the-art understanding-only and unified LVLMs in a zero-shot setting. We employ prompting strategies to guide each model to describe features region-by-region, predict corresponding bounding boxes, generate localized images (for unified models), and ultimately synthesize these findings into a complete radiology report.

**Evaluation Metrics.** We evaluate report quality using NLG and CE Metrics. To evaluate the interleaved multimodal reasoning capabilities of different LVLMs, we introduce Consistency Metric (Consist. Metric). This metrics comprise three distinct components: **(1) Generation Consistency (Gen.)**, which

evaluates the alignment between the model’s generative and grounding outputs by comparing the generated localized images against images extracted via the predicted bounding boxes using the structural similarity index measure (SSIM); **(2) Grounding Consistency (Grd.)**, which measures the spatial accuracy of the grounding mechanism by calculating the Mean Intersection over Union (mIoU) between the images extracted via predicted bounding boxes and the ground truth localized images; and **(3) Semantic Consistency (Sem.)**, which assesses the semantic quality of the multimodal CoT. This metric is defined as the sum of the semantic similarity between the localized textual descriptions and the generated localized images, and the semantic similarity between the generated localized images and the images extracted via the predicted bounding boxes using BiomedCLIP [30]. All experiments are conducted on a single NVIDIA H800 GPU.

**Results and Analysis.** Table 3 presents a comparative analysis of our model against advanced LVLMs. Our model achieves the highest performance across nearly all metrics, particularly in the Unified Large Language Model category. In terms of consistency metrics, our model attains a generation consistency of 0.482, a grounding consistency of 0.643, and a semantic consistency of 1.226, which exceeds other unified models such as UniMedVL [21]. This indicates that training based on MMRad-IVL-22K allows the model to generate accurate and consistent visual rationales and textual descriptions. This transparency in the reasoning process ensures that the diagnostic conclusions are grounded in verifiable visual evidence. Finally, the fidelity of these visual and textual rationales serves as a solid foundation for the report generation task, directly contributing to the production of higher-quality radiology reports.

**Evaluation of Clinical Application.** The proposed framework averages approximately 2 minutes per case for the full inference cycle (benchmarked on a single NVIDIA H800 GPU). A detailed profiling of this latency indicates that while textual diagnostic inference is nearly instantaneous, the bulk of the processing time is consumed by the autoregressive sampling of discrete visual tokens required to generate localized images. While this latency may preclude real-time intraoperative use, it remains highly compatible with standard asynchronous clinical workflows. In typical radiology practice, the median turnaround time from the appearance of examination results in PACS (Picture Archiving and Communication System) to the completion of a report by radiologist often exceeds 30 minutes [10]. Our model can operate as a background service integrated into the PACS, pre-computing reports and corresponding rationales during this interval. Furthermore, the 7B parameter footprint ensures that hospitals can deploy the system on mid-range consumer GPUs without specialized high-performance clusters. We anticipate that integrating efficiency-oriented techniques (such as speculative decoding) could further reduce the generation time.

### 3.3 Case Study

Figure 3 illustrates the model’s systematic diagnostic trace on a representative chest X-ray. The model first examines the mediastinal region by generating a

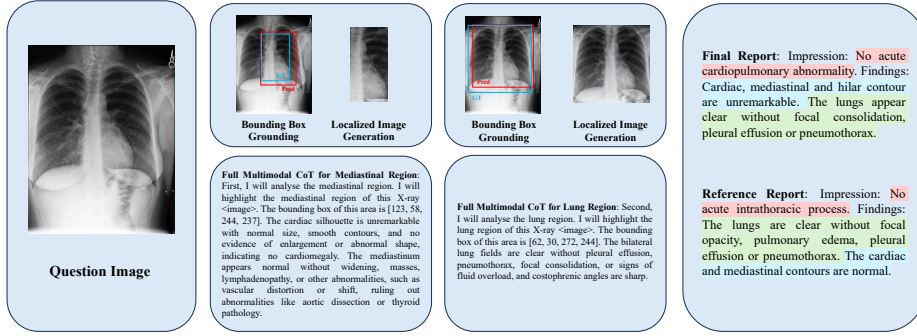


**Fig. 3. Qualitative analysis of the interleaved reasoning process and final report generated by Anole-RadCoT.** This systematic trace demonstrates high clinical fidelity through precise visual grounding. Green shading and blue shading represent consistent descriptions for the mediastinal and lung regions; red shading indicates partial consistency with similar meanings.

localized visual rationale and textual reasoning that rules out cardiac and mediastinal abnormalities. It then transitions to the lung region where it identifies clear lung fields with high spatial accuracy as evidenced. This multi-step process ensures that each diagnostic statement is grounded in verifiable visual evidence. The final report closely aligns with the reference report.

## 4 Conclusion

In this work, we introduce MMRad-IVL-22K, the first large-scale dataset designed to facilitate natively interleaved vision language reasoning in chest X-ray interpretation. MMRad-IVL-22K reflects a repeated cycle of reasoning and visual inspection workflow of radiologists. Extensive experiments on both advanced closed-source and open-source LVLMs demonstrate that this multimodal CoT strategy outperforms text-only CoT baselines, and model trained on our dataset yield gains in diagnostic transparency, reasoning consistency and report quality. These results confirm that high-fidelity interleaved visual evidence is a non-substitutable component of reliable medical AI. Therefore, MMRad-IVL-22K offers a scalable path toward the next generation of trustworthy and unified medical foundation models.

## References

1. Alkhaldi, A., Alnajim, R., Alabdullatef, L., Alyahya, R., Chen, J., Zhu, D., Alsinan, A., Elhoseiny, M.: Minigpt-med: Large language model as a general interface for radiology diagnosis. arXiv preprint arXiv:2407.04106 (2024)
2. Anthropic: Introducing claude haiku 4.5 (2025), <https://www.anthropic.com/news/clause-haiku-4-5>
3. Bae, S., Kyung, D., Ryu, J., Cho, E., Lee, G., Kweon, S., Oh, J., Ji, L., Chang, E., Kim, T., et al.: Ehrxqa: A multi-modal question answering dataset for electronic health records with chest x-ray images. Advances in Neural Information Processing Systems **36**, 3867–3880 (2023)
4. Bai, S., Chen, K., Liu, X., Wang, J., Ge, W., Song, S., Dang, K., Wang, P., Wang, S., Tang, J., et al.: Qwen2. 5-vl technical report. arXiv preprint arXiv:2502.13923 (2025)
5. Chern, E., Hu, Z., Chern, S., Kou, S., Su, J., Ma, Y., Deng, Z., Liu, P.: Thinking with generated images. arXiv preprint arXiv:2505.22525 (2025)
6. Deng, C., Zhu, D., Li, K., Gou, C., Li, F., Wang, Z., Zhong, S., Yu, W., Nie, X., Song, Z., et al.: Emerging properties in unified multimodal pretraining. arXiv preprint arXiv:2505.14683 (2025)
7. Google: Gemini 3 flash: frontier intelligence built for speed (2025), <https://blog.google/products-and-platforms/products/gemini/gemini-3-flash>
8. Google: Gemini 3 pro: the frontier of vision ai (2025), <https://blog.google/innovation-and-ai/technology/developers-tools/gemini-3-pro-vision/>
9. Hu, E.J., Shen, Y., Wallis, P., Allen-Zhu, Z., Li, Y., Wang, S., Wang, L., Chen, W., et al.: Lora: Low-rank adaptation of large language models. ICLR **1**(2), 3 (2022)
10. Hunter, J.G., Bera, K., Shah, N., Bukhari, S.M.A., Marshall, C., Caovan, D., Rosipko, B., Gupta, A.: Real-world performance of pneumothorax-detecting artificial intelligence algorithm and its impact on radiologist reporting times. Academic radiology **32**(3), 1165–1174 (2025)
11. Jain, S., Agrawal, A., Saporta, A., Truong, S.Q., Duong, D.N., Bui, T., Chambon, P., Zhang, Y., Lungren, M.P., Ng, A.Y., et al.: Radgraph: Extracting clinical entities and relations from radiology reports. arXiv preprint arXiv:2106.14463 (2021)
12. Jing, P., Lee, K., Zhang, Z., Zhou, H., Yuan, Z., Gao, Z., Zhu, L., Papanastasiou, G., Fang, Y., Yang, G.: Reason like a radiologist: Chain-of-thought and reinforcement learning for verifiable report generation. arXiv preprint arXiv:2504.18453 (2025)
13. Johnson, A.E., Pollard, T.J., Greenbaum, N.R., Lungren, M.P., Deng, C.y., Peng, Y., Lu, Z., Mark, R.G., Berkowitz, S.J., Horng, S.: Mimic-cxr-jpg, a large publicly available database of labeled chest radiographs. arXiv preprint arXiv:1901.07042 (2019)
14. Li, A., Wang, C., Fu, D., Yue, K., Cai, Z., Zhu, W.B., Liu, O., Guo, P., Neiswanger, W., Huang, F., et al.: Zebra-cot: A dataset for interleaved vision language reasoning. arXiv preprint arXiv:2507.16746 (2025)
15. Li, C., Wong, C., Zhang, S., Usuyama, N., Liu, H., Yang, J., Naumann, T., Poon, H., Gao, J.: Llava-med: Training a large language-and-vision assistant for biomedicine in one day. Advances in Neural Information Processing Systems **36**, 28541–28564 (2023)
16. Liu, A., Feng, B., Xue, B., Wang, B., Wu, B., Lu, C., Zhao, C., Deng, C., Zhang, C., Ruan, C., et al.: Deepseek-v3 technical report. arXiv preprint arXiv:2412.19437 (2024)

17. Liu, B., Zhao, X., He, A., Chen, Y., Fu, H., Wu, X.M.: Gemex-thinkvg: Towards thinking with visual grounding in medical vqa via reinforcement learning. arXiv preprint arXiv:2506.17939 (2025)
18. Liu, B., Zou, K., Zhan, L.M., Lu, Z., Dong, X., Chen, Y., Xie, C., Cao, J., Wu, X.M., Fu, H.: Gemex: A large-scale, groundable, and explainable medical vqa benchmark for chest x-ray diagnosis. In: Proceedings of the IEEE/CVF International Conference on Computer Vision. pp. 21310–21320 (2025)
19. Liu, K., Ma, Z., Kang, X., Li, Y., Xie, K., Jiao, Z., Miao, Q.: Enhanced contrastive learning with multi-view longitudinal data for chest x-ray report generation. In: Proceedings of the Computer Vision and Pattern Recognition Conference. pp. 10348–10359 (2025)
20. Nicolson, A., Dowling, J., Anderson, D., Koopman, B.: Longitudinal data and a semantic similarity reward for chest x-ray report generation. *Informatics in Medicine Unlocked* **50**, 101585 (2024)
21. Ning, J., Li, W., Tang, C., Lin, J., Ma, C., Zhang, C., Liu, J., Chen, Y., Gao, S., Liu, L., et al.: Unimedvl: Unifying medical multimodal understanding and generation through observation-knowledge-analysis. arXiv preprint arXiv:2510.15710 (2025)
22. North, Z.: How to interpret chest radiographs (x-rays): a systematic approach. *Nursing Times* **120**(6), 38–43 (2024)
23. OpenAI: Introducing gpt-5 (2025), <https://openai.com/index/introducing-gpt-5>
24. Wang, C., Sennrich, R.: On exposure bias, hallucination and domain shift in neural machine translation. arXiv preprint arXiv:2005.03642 (2020)
25. Wang, H., Ye, S., Lin, J., Naseem, U., Kim, J.: Lvmed-r2: Perception and reflection-driven complex reasoning for medical report generation. arXiv preprint arXiv:2504.02885 (2025)
26. Wang, P., Ye, S., Naseem, U., Kim, J.: Mrg-r1: Reinforcement learning for clinically aligned medical report generation. arXiv preprint arXiv:2512.16145 (2025)
27. Wang, W., Gao, Z., Gu, L., Pu, H., Cui, L., Wei, X., Liu, Z., Jing, L., Ye, S., Shao, J., et al.: Internvl3. 5: Advancing open-source multimodal models in versatility, reasoning, and efficiency. arXiv preprint arXiv:2508.18265 (2025)
28. Wu, Z., Chen, X., Pan, Z., Liu, X., Liu, W., Dai, D., Gao, H., Ma, Y., Wu, C., Wang, B., et al.: Deepseek-vl2: Mixture-of-experts vision-language models for advanced multimodal understanding. arXiv preprint arXiv:2412.10302 (2024)
29. Yang, A., Li, A., Yang, B., Zhang, B., Hui, B., Zheng, B., Yu, B., Gao, C., Huang, C., Lv, C., et al.: Qwen3 technical report. arXiv preprint arXiv:2505.09388 (2025)
30. Zhang, S., Xu, Y., Usuyama, N., Xu, H., Bagga, J., Tinn, R., Preston, S., Rao, R., Wei, M., Valluri, N., et al.: Biomedclip: a multimodal biomedical foundation model pretrained from fifteen million scientific image-text pairs. arXiv preprint arXiv:2303.00915 (2023)
31. Zhang, X., Wu, C., Zhao, Z., Lei, J., Zhang, Y., Wang, Y., Xie, W.: Radgenome-chest ct: A grounded vision-language dataset for chest ct analysis. arXiv preprint arXiv:2404.16754 (2024)